

Noise Diffusion for Enhancing Semantic Faithfulness in Text-to-Image Synthesis

Boming Miao
Beijing Normal University

Chunxiao Li
Beijing Normal University

Xiaoxiao Wang
University of Chinese Academy of Sciences

Andi Zhang
The University of Manchester

Rui Sun
The Chinese University of Hong Kong, Shenzhen

Zizhe Wang
Tsinghua University

Yao Zhu
Tsinghua University

Abstract

Diffusion models have achieved impressive success in generating photorealistic images, but challenges remain in ensuring precise semantic alignment with input prompts. Optimizing the initial noisy latent offers a more efficient alternative to modifying model architectures or prompt engineering for improving semantic alignment. A latest approach, InitNo, refines the initial noisy latent by leveraging attention maps; however, these maps capture only limited information, and the effectiveness of InitNo is highly dependent on the initial starting point, as it tends to converge on a local optimum near this point. To this end, this paper proposes leveraging the language comprehension capabilities of large vision-language models (LVLMs) to guide the optimization of the initial noisy latent, and introduces the Noise Diffusion process, which updates the noisy latent to generate semantically faithful images while preserving distribution consistency. Furthermore, we provide a theoretical analysis of the condition under which the update improves semantic faithfulness. Experimental results demonstrate the effectiveness and adaptability of our framework, consistently enhancing semantic alignment across various diffusion models. The code is available at <https://github.com/Bomingmiao/NoiseDiffusion>.

beddings from input prompts. Recent advancements have also focused on performing the diffusion process in a lower-dimensional latent space. This latent space is typically derived from a pre-trained encoder, such as a variational autoencoder (VAE) [15], which enhances both efficiency and image consistency.

Despite their success in generating high-quality images, diffusion models still face challenges in producing images that align with the description of the prompts. Improving diffusion models [2, 30, 33, 42] and implementing prompt engineering [3, 22, 26, 40] represent two well-established approaches to addressing this challenge. While the former typically involves substantial training costs, the latter, though capable of enhancing generation quality through refined input prompts, may occasionally diverge semantically from the original prompts. In contrast, optimizing latent input remains relatively underexplored. Chefer et al. [5] observe that cross-attention maps can reveal the degree of alignment between text prompts and generated images, and propose a method to optimize latent variables at each denoising step. Building on an in-depth examination of attention layers within diffusion models, Guo et al. [12] introduce InitNo, an approach that optimizes the initial noisy latent variables and outperforms existing methods in generating semantically accurate images.

However, the InitNo framework still faces two notable challenges. First, InitNo is effective only when the target point lies within the ℓ_∞ neighborhood of the initial point. This is because InitNo uses a gradient-based method to update the mean and variance of the latent variable, which may lead to a distribution shift. To prevent excessive deviation of the updated latent variable distribution from the standard Gaussian distribution, InitNo restricts its search for the optimal solution to a local region near the initial point. Second, the misalignment between the generated images and input prompts often arises from insufficient understanding of the prompt content and image components [19], suggesting that

1. Introduction

Diffusion models have become the dominant approach in text-to-image generation due to their exceptional performance in this area [30, 31, 33]. The core mechanism of diffusion models involves progressively adding noise to an image and using a neural network, such as U-Net [32] or DiT [27], to predict the noise and then remove it based on the prediction during the reverse process. In the latest diffusion models, denoising is guided by conditional text em-



Figure 1. Example results of Stable Diffusion models and ours. Given a fixed initial noisy latent, we optimize the latent toward an area that can generate images aligned with the input prompts.

relying solely on attention layers to improve alignment may have limited effectiveness.

In response to these challenges, this paper presents a novel framework for optimizing the initial noisy latent during the denoising process. To improve the generation process’s understanding of image components and prompt content, we employ a large vision-language model (LVLM) for supervision. Specifically, the image generated by the diffusion model, along with a question derived from the prompt, is input into the LVLM to compute the Visual Question Answering (VQA) score proposed by [18]. We then optimize the latent variable to maximize this score to ensure better alignment between the generated image and the prompt. Regarding the preservation of distribution consistency during latent variable optimization, we introduce the Noise Diffusion method. This approach applies the diffusion forward process to update the latent variable, progressively adding Gaussian noise to the original latent variable, shifting it to a region conducive to generating more semantically consistent and satisfactory images. The challenge with this method lies in determining the optimal noise that can increase the VQA score, as existing methods are ineffective in using gradient information to sample Gaussian noise. To address this, we sample a set of noises at each iteration, compute the step difference based on the pre-defined step size and the sampled noise, and utilize gradient information to select the most appropriate step difference for updating the latent variable. We theoretically prove that when the ratio of the inner product of the step difference and gradient to the square of the step difference’s norm exceeds a threshold, the optimization will increase the VQA score. As shown in Fig. 1, when the vanilla Stable Diffusion (SD) model fails to produce images that align with the prompt, our method for refining the latent variable ensures better alignment between the generated images and the prompts. Our contributions are summarized as follows:

- We propose a novel framework that harnesses the semantic understanding of LVLMs to supervise the diffusion generation process and introduces the Noise Diffusion

method to optimize the initial noisy latent variables while preserving the distribution of the latent variables, thereby enhancing the semantic faithfulness of the generated images to the input prompts.

- We provide a theoretical analysis of the condition under which updating the latent variables can increase the VQA score. Based on this analysis, we propose a strategy for selecting the noise for update process using gradient information.
- Extensive experimental results demonstrate the superiority of our method, which can seamlessly and effectively enhance the semantic faithfulness of various diffusion models.

2. Related Work

Early studies on text-to-image synthesis mainly focus on GANs [39, 41, 44–46] and auto-regressive models [4, 9, 29, 43]. More recently, diffusion models have outperformed these methods [8]. The concept of training a generative model by adding noise to data and learning the reverse process to restore the original data distribution is first proposed by [36]. DDPM [14] showcases the remarkable ability of diffusion models for unconditional image generation. Song et al. [38] extend this by presenting a stochastic differential equation (SDE) to model the forward and reverse processes, and derive an equivalent neural ordinary differential equation (ODE) that samples from the same distribution, enabling exact likelihood computation and improving sampling efficiency. To achieve photorealism in class-conditional settings, Dhariwal and Nichol [8] enhance diffusion models with classifier guidance by training a classifier on noisy images and using its gradients to guide samples toward the target label. Ho and Salimans [13] introduce classifier-free guidance, which combines the score estimates from a jointly trained conditional and unconditional model. For generating images from free-form textual prompts, Nichol et al. [25] employ a text encoder to condition the denoising process on language descriptions, and demonstrate that text-guided diffusion models with classifier-free guidance can yield higher quality images.

Meanwhile, numerous efforts have been made to address the issue of unfaithfulness in image generation using diffusion models. One research direction is to explore how to train more powerful diffusion models. Balaji et al. [2] observe the difference of the importance of the text condition in different denoising stages and propose training an ensemble of text-to-image diffusion models specialized for different synthesis stages. Ramesh et al. [30] enhance the output of diffusion models with prior CLIP image embeddings added to the timestep embedding of diffusion models and concatenated with the output of text encoder. Saharia et al. [33] enhance the alignment of textual and visual content with the language understanding of large language

models (LLMs). Xue et al. [42] introduce stacking tens of mixture-of-experts (MoEs) layers to generate highly artistic images. Segalis et al. [34] point out relabeling the corpus with a specialized automatic captioning model can significantly improve the quality of the dataset for training a diffusion model.

Another line of works explore strategies without retraining or modifying the models. Liu et al. [21] propose generating an image with a set of diffusion models, each of which model a certain component of the image. Si et al. [35] observe differences in feature contributions between the U-Net architecture’s main backbone and its skip connections, and improve the generation quality by introducing two specialized modulation factors for the feature maps in these respective components. Feng et al. [11] propose splitting the input text prompts and manipulating the cross-attention representations to better preserve the compositional semantics. Chefer et al. [5] introduce the concept of Generative Semantic Nursing (GSN), intervening in the denoising process by optimizing the latent at each timestep to refine the cross-attention, so as to encourage generating all subjects described in the text prompt. Agarwal et al. [1], Li et al. [17] further improve the optimization objective for better update direction. Guo et al. [12] point out that optimizing the noisy latent at each denoising timestep requires carefully designed parameters and is hard to control the extent of optimization, and propose an alternative method by adjusting the sampled noise in the initial latent space.

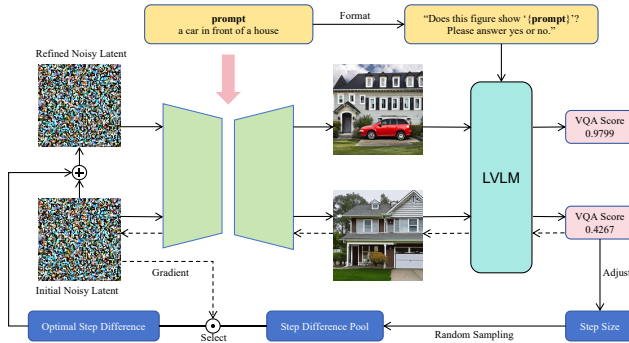


Figure 2. The framework of Noise Diffusion. The image generated from the initial noisy latent is fed into the LVLM along with a question formatted as, “Does this figure show ‘{prompt}’? Please answer yes or no.” The probability of the token “Yes” serves as the VQA score. The step size for updating the noisy latent is dynamically adjusted based on the score value. Gradient information is then used to select the optimal noise for the update according to the step difference.

3. Method

3.1. Preliminary

VQA Score. We utilize VQA score proposed by [18] to measure the alignment between generated images and input prompts. The image I is input into a large vision-language model along with the question: “Does this figure show ‘{prompt}’? Please answer yes or no.” The VQA score is then computed as:

$$VQA(I, \text{prompt}) = P(\text{“Yes”} \mid I, \text{prompt}). \quad (1)$$

Diffusion Models. For diffusion process in latent space, the noise is added progressively through a variance schedule β_1, \dots, β_T . Let $\alpha_t := 1 - \beta_t$, $\bar{\alpha}_t := \prod_{s=1}^t \alpha_s$, the noisy latent can be expressed as:

$$q(z_t \mid z_0) = \mathcal{N}(z_t; \sqrt{\bar{\alpha}_t} z_0, (1 - \bar{\alpha}_t) \mathbf{I}) \quad (2)$$

For text-to-image synthesis, the denoising process begins from the initial latent variable z_T . Let \mathcal{C} denote the text embedding and \emptyset denote the null embedding, the classifier-free noise prediction can be expressed as:

$$\epsilon_\theta(z_t, t, \mathcal{C}, \emptyset) = w \cdot \epsilon_\theta(z_t, t, \mathcal{C}) + (1-w) \cdot \epsilon_\theta(z_t, t, \emptyset), \quad (3)$$

where w denotes the guidance scale parameter, which is fixed as 7.5 in Stable Diffusion models. For simplicity, we use $\epsilon_\theta(z_t)$ to represent $\epsilon_\theta(z_t, t, \mathcal{C}, \emptyset)$. Since noisy latent optimization requires a deterministic denoising process, we adopt DDIM [37] to ensure consistency across the iterations. In the DDIM framework, the noisy latent from the previous timestep can be obtained by:

$$z_{t-1} = \sqrt{\frac{\alpha_{t-1}}{\alpha_t}} (z_t - \sqrt{1 - \alpha_t} \epsilon_\theta(z_t)) + \sqrt{1 - \alpha_{t-1}} \epsilon_\theta(z_t). \quad (4)$$

After completing the denoising process, a decoder $\mathcal{D}(\cdot)$ is applied to the final denoised latent z_0 to generate the output image I : $I = \mathcal{D}(z_0)$.

Gradient Approximation. In our pipeline, z_T is denoised to z_0 , and z_0 is decoded into image I , which is fed to the LVLM to compute the VQA score. Therefore the score of z_T can be defined as:

$$s(z_T) = VQA(\mathcal{D}(\Omega(z_T, \mathcal{C}, \emptyset)), \text{prompt}), \quad (5)$$

where Ω denotes the DDIM denoising process. The gradient of the objective with respect to z_T can be computed as:

$$\nabla_{z_T} s(z_T) = \frac{\partial s(z_T)}{\partial I} \frac{\partial I}{\partial z_0} \frac{\partial z_0}{\partial z_T}, \quad (6)$$

where $\frac{\partial z_0}{\partial z_T}$ constitutes the primary computational cost, as it requires back propagation through multiple timesteps in the

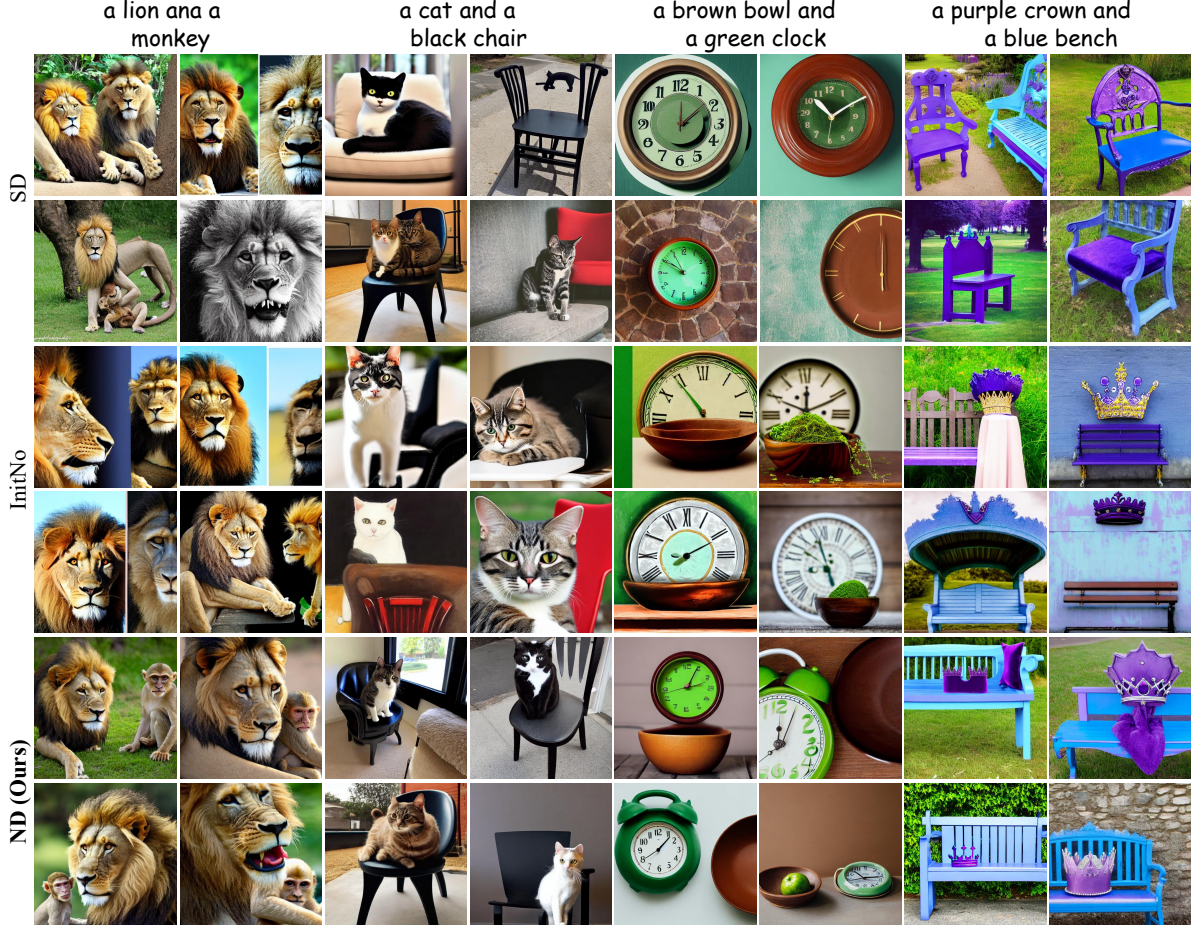


Figure 3. Qualitative comparison for simple cases. Each image is generated with the same prompt and random seed for all methods. The images generated by our method contain objects that most closely match the features described in the prompts.

denoising process. The derivative of the latent variable at the previous timestep with respect to the current timestep is given by:

$$\frac{\partial z_{t-1}}{\partial z_t} = \sqrt{\frac{\alpha_{t-1}}{\alpha_t}} + \sqrt{\frac{\alpha_t - \alpha_{t-1}}{\alpha_t}} \frac{\partial \epsilon_\theta(z_t)}{\partial z_t}. \quad (7)$$

According to the chain rule, $\frac{\partial z_0}{\partial z_T}$ can be expanded as:

$$\begin{aligned} \frac{\partial z_0}{\partial z_T} &= \left(\sqrt{\frac{\alpha_0}{\alpha_1}} + \sqrt{\frac{\alpha_1 - \alpha_0}{\alpha_1}} \frac{\partial \epsilon_\theta(z_1)}{\partial z_1} \right) \frac{\partial z_1}{\partial z_2} \dots \frac{\partial z_{T-1}}{\partial z_T} \\ &= \left(\sqrt{\frac{\alpha_0}{\alpha_1}} \frac{\partial z_1}{\partial z_2} + \sqrt{\frac{\alpha_1 - \alpha_0}{\alpha_1}} \frac{\partial \epsilon_\theta(z_1)}{\partial z_2} \right) \frac{\partial z_2}{\partial z_3} \dots \frac{\partial z_{T-1}}{\partial z_T} \\ &= \sqrt{\frac{1}{\alpha_T}} + \sum_{i=1}^T \sqrt{\frac{\alpha_i - \alpha_{i-1}}{\alpha_{i-1} \alpha_i}} \frac{\partial \epsilon_\theta(z_i)}{\partial z_T}, \end{aligned} \quad (8)$$

where $\alpha_0 = 1$. The computational cost of the full process is extremely high. To simplify the calculation, we adopt the simple approximation proposed by [24], where $\epsilon_\theta(z_t)$

is treated as a constant ϵ_t for all $t = 1, \dots, T$. In this way $\frac{\partial \epsilon_\theta(z_t)}{\partial z_T} = 0$ since $\epsilon_\theta(z_t)$ is assumed to be independent to z_T . Consequently, we have $\frac{\partial z_0}{\partial z_T} = \sqrt{\frac{1}{\alpha_T}}$. Therefore the gradient calculation can be simplified as:

$$\nabla_{z_T} s(z_T) = \sqrt{\frac{1}{\alpha_T}} \frac{\partial s(z_T)}{\partial I} \frac{\partial I}{\partial z_0}. \quad (9)$$

3.2. Noise Diffusion

We use the same approach as the diffusion forward process to transfer the initial noisy latent to a new state. Specifically, for the current latent z_T , the updated latent z'_T is obtained by:

$$z'_T = \sqrt{1 - \gamma} z_T + \sqrt{\gamma} \sigma, \quad (10)$$

where $\sigma \sim \mathcal{N}(0, \mathbf{I})$, γ is the step size. Since z_T and σ both cohere to standard Gaussian distribution, the updated latent $z'_T \sim \mathcal{N}(0, \mathbf{I})$ holds true, regardless of the value of γ . This allows us to obtain a latent that is distant from the original while remaining in the same distribution.

Score-Aware Step Size. The step size determines the magnitude of the perturbation to the latent variable. Considering that the step size should be large when the score is low, and small when the score is high, we employ the following function to dynamically adjust the step size:

$$\gamma = 1 - \sqrt{s(z_T)}. \quad (11)$$

Algorithm 1 Noise Diffusion

Require: A prompt P , a pretrained diffusion model and LVLm, number of denoising steps T , initial latent at the last timestep z_T , max optimization epoch M , number of candidate noises N .

Ensure: The refined image

- 1: $\mathcal{C}, \emptyset \leftarrow \text{TextEncoder}(P, \text{" "})$.
 - 2: $I \leftarrow \mathcal{D}(\Omega(z_T, \mathcal{C}, \emptyset))$.
 - 3: Calculate $s(z_T)$ based on Eq. (5).
 - 4: $I^* \leftarrow I, s^* \leftarrow s(z_T)$.
 - 5: **for** $m = 1, \dots, M$ **do**
 - 6: $\gamma = 1 - \sqrt{s(z_T)}$.
 - 7: Calculate $\nabla_{z_T} s(z_T)$ based on Eq. (9).
 - 8: Randomly sample a set of noises $[\sigma_1, \dots, \sigma_N]$.
 - 9: $v_i = (\sqrt{1 - \gamma} - 1)z_T + \sqrt{\gamma}\sigma_i, i = 1, \dots, N$.
 - 10: $\sigma = \arg \max_{i \in [1, \dots, N]} \nabla_{z_T} s(z_T) v_i / \|v_i\|_2^2$.
 - 11: $z_T \leftarrow \sqrt{1 - \gamma}z_T + \sqrt{\gamma}\sigma$.
 - 12: $I \leftarrow \mathcal{D}(\Omega(z_T, \mathcal{C}, \emptyset))$.
 - 13: **if** $s(z_T) > s^*$ **then**
 - 14: $s^* \leftarrow s(z_T), I^* \leftarrow I$.
 - 15: **end if**
 - 16: **end for**
 - 17: **return** I^*
-

Noise Selection. Let v denote the step difference between z_T and z'_T obtained by Eq. (10). v can be expressed as:

$$v = (\sqrt{1 - \gamma} - 1)z_T + \sqrt{\gamma}\sigma. \quad (12)$$

For simplicity, we regard z_T as a vector, the score of updated latent variable $s(z'_T)$ can be expressed in Taylor expansion:

$$s(z'_T) = s(z_T) + \nabla_{z_T} s(z_T)v + \frac{1}{2}v^T \nabla_{\xi}^2 s(\xi)v, \quad (13)$$

where $\xi = z_T + \rho v, \rho \in (0, 1)$. Therefore, $\nabla_{z_T} s(z_T)v$ plays an important role in determining the value of $s(z'_T)$. Randomly sampling noise σ from a Gaussian distribution may not guarantee that $\nabla_{z_T} s(z_T)v$ is positive, and thus this may not guarantee an overall increase in the score. To ensure that the overall update process progresses toward regions with higher VQA scores, we use the gradient information to select the appropriate noise for updating. As presented in Alg. 1, once the step size is obtained based on

the score and the gradient is computed, we then sample a set of candidate noises, and select the noise that maximizes $\nabla_{z_T} s(z_T)v / \|v\|_2^2$. Finally, we update z_T using the selected noise by Eq. (10). We provide an overview of our proposed Noise Diffusion method in Fig. 2.

Feasibility Analysis. To obtain a latent that yields a higher score after iterations, the noise for updating z_T must satisfy the certain condition. Existing widely adopted activation functions in neural networks have bounded second derivatives almost everywhere [10]. So there exists a positive constant c so that for any given ξ ,

$$\|\nabla_{\xi}^2 s(\xi)\|_2 \stackrel{\text{a.e.}}{\leq} c \quad (14)$$

is satisfied. Then if the condition $\nabla_{z_T} s(z_T)v / \|v\|_2^2 \geq \frac{c}{2} + \delta, \delta > 0$ holds true, we can obtain that

$$\begin{aligned} s(z'_T) &= s(z_T) + \nabla_{z_T} s(z_T)v + \frac{1}{2}v^T \nabla_{z_T}^2 s(\xi)v \\ &\stackrel{\text{a.e.}}{\geq} s(z_T) + \nabla_{z_T} s(z_T)v - \frac{c}{2}\|v\|_2^2 \\ &\geq s(z_T) + \frac{c + \delta}{2}\|v\|_2^2 - \frac{c}{2}\|v\|_2^2 \\ &= s(z_T) + \delta\|v\|_2^2. \end{aligned} \quad (15)$$

Therefore, maximizing $\nabla_{z_T} s(z_T)v / \|v\|_2^2$ is effective in identifying the noise that satisfies the condition for updating towards a higher score.

4. Experiment

4.1. Implementation Details

Model Choice. In accordance with [12], we utilize the official Stable Diffusion V-1.4 [31] as the base diffusion model alongside CLIP-FlanT5-11B [18] to compute the VQA score in Sec. 4.2, Sec. 4.3 and Sec. 4.4. In Sec. 4.5, we evaluate the effectiveness and generalization capability of our method across various diffusion models, including Stable Diffusion V-1.5, V-2.0, and V-2.1, as well as several LVLms, such as InstructBLIP-FlanT5-11B [7], LLaVA-1.5-13B [20], and ShareGPT4V-13B [6]. We compute the CLIP score using the CLIP ViT-L/14 model [28].

Hyper-parameters. The number of denoising steps T , max optimization epoch M and candidate noises N are all set as 50. Evaluated on a single NVIDIA RTX A6000 (48GB), SD V-1.4 synthesizes an image in an average of 6.08 seconds, while our method requires additional 6.71 seconds for one optimization epoch. Although our method requires additional computational cost, it significantly improves the semantic faithfulness of the generated images. Moreover, choosing smaller hyper-parameters can also reduce the computational cost. We discuss the impact of hyper-parameters in the Appendix. B.

Datasets. We use two prompt datasets, covering simple and complex cases to evaluate the alignment of prompts and



Figure 4. Qualitative comparison for complex cases. Each image is generated with the same text prompt and random seed for all methods. Our method exhibits strong understanding of the positional relationships described in the prompts.

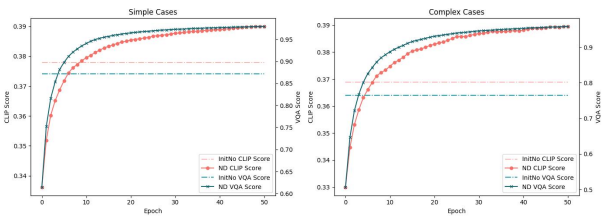


Figure 5. The average CLIP score and VQA score of the generated images both increase as the epochs progress and eventually converge. Compared to InitNo, the Noise Diffusion (ND) method consistently outperforms InitNo in both CLIP and VQA scores.

images. The simple cases focus on object structures and are sourced from the dataset proposed by [5]. For complex cases, we retain the objects from the simple cases, randomly replacing conjunctions such as “and” or “with” with spatial terms like “on,” “under,” “above,” or “below” to represent positional relationships. See the Appendix. C for detailed descriptions of the datasets.

4.2. Qualitative Comparison

Fig. 3 and Fig. 4 illustrate a comparison between our proposed method, Stable Diffusion (SD) and InitNo under simple and complex cases, respectively. With identical prompts and seeds, our method demonstrates clear advantages over the other approaches. In Fig. 3, we observe that images generated by the vanilla Stable Diffusion model may exhibit issues such as object blending, object omission, or color distortion. In mitigating these deficiencies, our method demonstrates clear superiority over the existing state-of-the-art approach, InitNo. Specifically, in the case of the prompt “a lion and a monkey,” where SD fails to render the “monkey,” InitNo also struggles to capture the features of the monkey.

In contrast, our method encourages the diffusion model to generate a harmonious image containing both the lion and the monkey. Furthermore, with the prompt “a brown bowl and a green clock,” while InitNo successfully outlines the structures of the bowl and the clock, it frequently misinterprets their colors. Our method, however, exhibits more effective performance in accurately rendering the colors.

When we introduce more complex cases, we find that although InitNo may succeed in rendering the structure of the objects described in the prompts, it fails to capture the underlying logic, leading to a significant deviation from the required semantics. For example, with the prompt “a blue egg on a rabbit,” SD fails to depict a rabbit. While InitNo successfully presents both a rabbit and a blue egg, it completely overlooks the concept of “on,” resulting in an image of “a blue egg beside a rabbit.” In contrast, our method effectively adjusts the relationship between the rabbit and the egg, demonstrating the advantage of incorporating feedback from the LVLM to refine image generation.

4.3. Quantitative Comparison

To evaluate the effectiveness of our proposed method, we conduct quantitative comparative experiments on two datasets. For each prompt, we randomly select 25 seeds. To reflect the changes in semantic faithfulness during the optimization process of our method, we plot the average VQA and CLIP scores of the generated images at different epochs across two datasets in Fig. 5. Additionally, we also present the average VQA and CLIP scores after optimization using the InitNo method for comparison. Both the VQA score and the CLIP score of the generated images show an ascending trend over time. At epoch 0, the images are generated using the unoptimized Vanilla SD model. On datasets with simple cases, when the optimization epoch reaches 10, our method



Figure 6. We compare different optimization methods using the prompt “a bear wearing a T-shirt” as an example. PGD and Mean-Variance can only converge to a local optimum. Random Sampling searches for the optimal point randomly and proves ineffective. Random Diffusion improves upon Random Sampling by introducing an adjusted step size, making it more effective. However, Noise Diffusion outperforms all other methods, efficiently producing an image that closely matches the prompt.

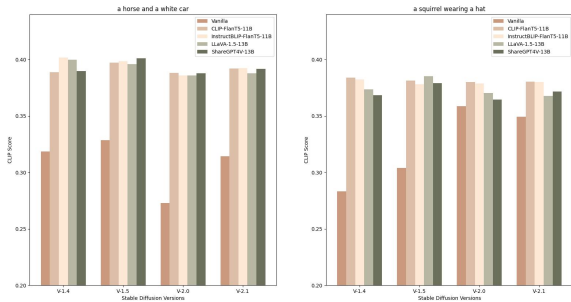


Figure 7. Comparison of the average CLIP score of images generated by different SD models and refined by various LVLMs.

achieves a VQA score of 0.9352, surpassing the average VQA score of InitNo (0.8717). As the optimization epoch approaches 50, the performance improvements brought by our method begin to plateau, with the VQA score reaching 0.9790, exceeding the average VQA score of InitNo by 0.1073. On datasets with complex cases, the performance advantage of our method is even more pronounced. At epoch 10, our method achieves a VQA score of 0.8791, surpassing the average VQA score of InitNo by 0.1144. As the optimization epoch approaches 50, our method achieves a VQA score of 0.9578, again surpassing the average VQA score of InitNo by 0.1930. This underscores the clear advantages of our method in handling complex semantic information.

4.4. Comparison of Different Optimization Techniques

Our method consists of two key components. The first is the adoption of a large vision-language model to refine the generation, which as discussed earlier, demonstrates the superior ability to capture the detail of images. The second part is the proposed Noise Diffusion method. To highlight the advantages of our proposed optimization technique, we examine a specific example using the prompt “a bear wearing a T-shirt.” As shown in Fig. 6, we present the images generated by the optimized noisy latent at different epochs. Among these comparative methods, Mean-Variance refers to the perturbation method used in InitNo, where the mean and variance of the Gaussian distribution are adjusted using Adam optimizer [16]. For a comprehensive comparison, we also introduce the PGD method [23], which directly perturbs the latent, as well as Random Sampling, where we randomly select another noise to replace the current noise at each timestep. Additionally, we introduce Random Diffusion, where the step size is determined by the VQA score, but the noise is randomly sampled for optimization rather than being guided by the gradient as in our proposed Noise Diffusion. As illustrated in Fig. 6, the content in the initial image deviates significantly from the prompt description. Methods like PGD, which directly perturbs the latent, or Mean-Variance, which perturbs the mean and variance based on gradients, show limited changes to the image structure, with relatively small visual adjustments. By the 50th epoch, the visual quality of images produced by the Mean-Variance method has notably declined. This sug-

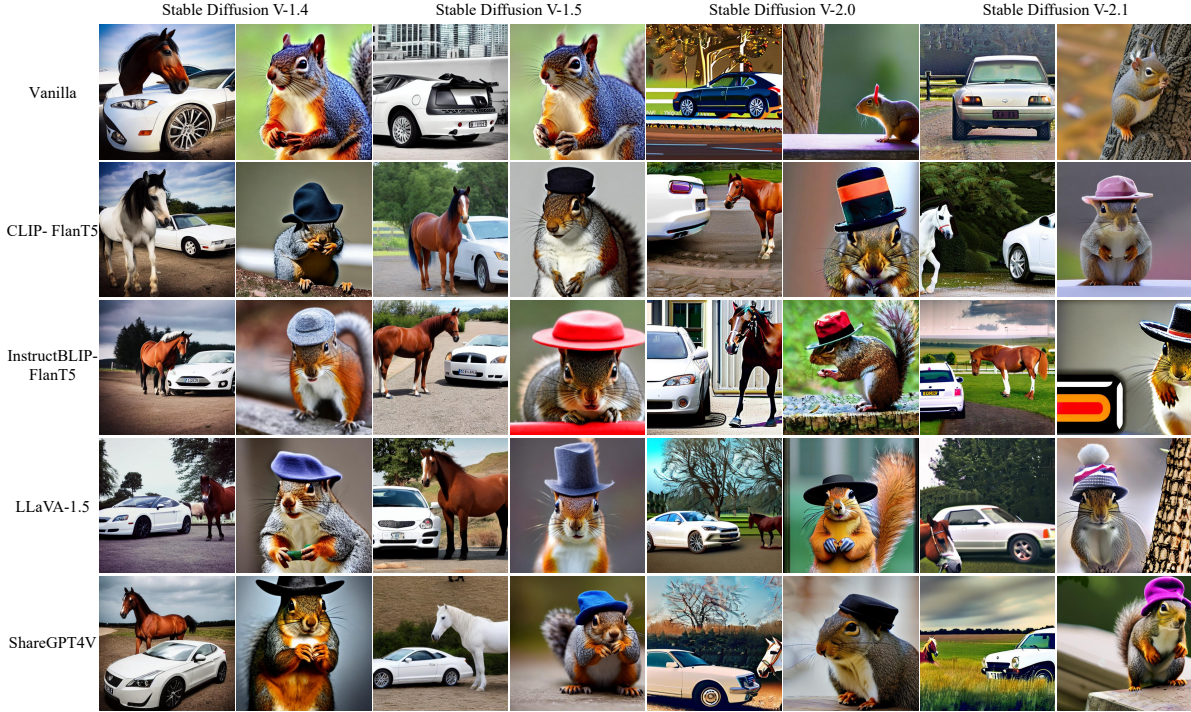


Figure 8. We use the prompts “a horse and a white car” and “a squirrel wearing a hat” as examples, conducting experiments on Stable Diffusion V-1.4, V-1.5, V-2.0, and V-2.1. We apply CLIP-FlanT5-11B, InstructBLIP-FlanT5-11B, LLaVA-1.5-13B, and ShareGPT4V-13B as the LVLMs for refining the generation. The faithfulness of image generation improves across all combinations of models.

gests that the initial latent lies in a low-score region within the noise space, and there are no nearby points with significantly higher scores. Consequently, this optimization faces limitations due to the trade-off between visual quality and perturbation extent, making it challenging to achieve substantial improvement. In contrast, methods such as Random Sampling, Random Diffusion, and our proposed Noise Diffusion demonstrate global optimization. Compared to the initial image, the appearance of the bear evolves considerably over subsequent epochs. Random Sampling, which operates with a fixed step size of 1 at each iteration, depends on the proportion of the latent space that yields favorable images. If this proportion is low, Random Sampling becomes highly inefficient. Random Diffusion enhances this approach by introducing a dynamic step size adjustment based on the VQA score. Although still not fully matching the prompt, the images generated by Random Diffusion align better with the prompt compared to those produced by Random Sampling. This validates the advantage of our step size adjustment method based on the score. Comparing Random Diffusion with Noise Diffusion, we observe that Noise Diffusion produces an image closely matching the prompt as early as epoch 5, and this result remains stable. This demonstrates the efficiency gained by incorporating gradient information into the update process.

4.5. Impact of Models

To evaluate the generalization capability of our method, we conduct experiments to assess the impact of different model configurations on the results. Specifically, we use CLIP-FlanT5-11B, InstructBlip-FlanT5-13B, LLaVA-1.5-13B and ShareGPT4V-13B to refine the text-to-image synthesis outputs of SD models V-1.4, V-1.5, V-2.0, and V-2.1. For evaluation, we select two prompts—“a horse and a white car” as a simple case and “a squirrel wearing a hat” as a complex case—and generate images using 25 randomly selected seeds. As shown in Fig. 7, the average CLIP scores of the generated images refined by LVLMs exceeds those of the vanilla settings, demonstrating that our method improves performance across all the models used, validating its effectiveness and generalization capability. Fig. 8 highlights that SD fails to generate the concept of “horse” in the prompt “a horse and a white car” and “hat” in the prompt “a squirrel wearing a hat.” In contrast, the refined images successfully present the missing objects, further emphasizing the effectiveness of our optimization approach.

5. Conclusion

This paper proposes a novel framework that leverages the capabilities of large vision-language models (LVLMs) in image components and textual semantic understanding to

optimize the initial noisy latent variables, thereby enhancing the semantic faithfulness of text-to-image synthesis. Specifically, we employ the Visual Question Answering (VQA) score to assess the alignment between the generated image and the textual prompt. Additionally, we introduce a noise diffusion approach, which updates the latent variables through a forward diffusion process, dynamically adjusting the step size and selecting the optimal noise for latent variable update based on the approximate gradient of the VQA score. We theoretically analyze the condition under which the update can enhance the VQA score. Our approach surpasses the current state-of-the-art in generating semantically faithful images, offering a flexible, plug-and-play solution compatible with existing diffusion models for training-free controllable generation.

References

- [1] Aishwarya Agarwal, Srikrishna Karanam, KJ Joseph, Apoorv Saxena, Koustava Goswami, and Balaji Vasanth. A-star: Test-time attention segregation and retention for text-to-image synthesis. In *Proceedings of the IEEE/CVF International Conference on Computer Vision*, pages 2283–2293, 2023. 3
- [2] Yogesh Balaji, Seungjun Nah, Xun Huang, Arash Vahdat, Jiaming Song, Qinsheng Zhang, Karsten Kreis, Miika Aittala, Timo Aila, Samuli Laine, et al. ediff-i: Text-to-image diffusion models with an ensemble of expert denoisers. *arXiv preprint arXiv:2211.01324*, 2022. 1, 2
- [3] Stephen Brade, Bryan Wang, Mauricio Sousa, Sageev Oore, and Tovi Grossman. Promptify: Text-to-image generation through interactive prompt exploration with large language models. In *Proceedings of the 36th Annual ACM Symposium on User Interface Software and Technology*, pages 1–14, 2023. 1
- [4] Huiwen Chang, Han Zhang, Jarred Barber, AJ Maschinot, Jose Lezama, Lu Jiang, Ming-Hsuan Yang, Kevin Murphy, William T Freeman, Michael Rubinstein, et al. Muse: Text-to-image generation via masked generative transformers. *arXiv preprint arXiv:2301.00704*, 2023. 2
- [5] Hila Chefer, Yuval Alaluf, Yael Vinker, Lior Wolf, and Daniel Cohen-Or. Attend-and-excite: Attention-based semantic guidance for text-to-image diffusion models. *ACM Transactions on Graphics (TOG)*, 42(4):1–10, 2023. 1, 3, 6
- [6] Lin Chen, Jinsong Li, Xiaoyi Dong, Pan Zhang, Conghui He, Jiaqi Wang, Feng Zhao, and Dahua Lin. Sharegpt4v: Improving large multi-modal models with better captions. *arXiv preprint arXiv:2311.12793*, 2023. 5
- [7] Wenliang Dai, Junnan Li, Dongxu Li, Anthony Meng Huat Tiong, Junqi Zhao, Weisheng Wang, Boyang Li, Pascale Fung, and Steven Hoi. Instructblip: Towards general-purpose vision-language models with instruction tuning, 2023. 5
- [8] Prafulla Dhariwal and Alexander Nichol. Diffusion models beat gans on image synthesis. *Advances in neural information processing systems*, 34:8780–8794, 2021. 2
- [9] Ming Ding, Zhuoyi Yang, Wenyi Hong, Wendi Zheng, Chang Zhou, Da Yin, Junyang Lin, Xu Zou, Zhou Shao, Hongxia Yang, et al. Cogview: Mastering text-to-image generation via transformers. *Advances in neural information processing systems*, 34:19822–19835, 2021. 2
- [10] Shiv Ram Dubey, Satish Kumar Singh, and Bidyut Baran Chaudhuri. Activation functions in deep learning: A comprehensive survey and benchmark. *Neurocomputing*, 503: 92–108, 2022. 5
- [11] Weixi Feng, Xuehai He, Tsu-Jui Fu, Varun Jampani, Arjun Akula, Pradyumna Narayana, Sugato Basu, Xin Eric Wang, and William Yang Wang. Training-free structured diffusion guidance for compositional text-to-image synthesis. *arXiv preprint arXiv:2212.05032*, 2022. 3
- [12] Xiefan Guo, Jinlin Liu, Miaomiao Cui, Jiankai Li, Hongyu Yang, and Di Huang. Initno: Boosting text-to-image diffusion models via initial noise optimization. In *Proceedings of the IEEE/CVF Conference on Computer Vision and Pattern Recognition*, pages 9380–9389, 2024. 1, 3, 5
- [13] Jonathan Ho and Tim Salimans. Classifier-free diffusion guidance. *arXiv preprint arXiv:2207.12598*, 2022. 2
- [14] Jonathan Ho, Ajay Jain, and Pieter Abbeel. Denoising diffusion probabilistic models. *Advances in neural information processing systems*, 33:6840–6851, 2020. 2
- [15] Diederik P Kingma. Auto-encoding variational bayes. *arXiv preprint arXiv:1312.6114*, 2013. 1
- [16] Diederik P Kingma. Adam: A method for stochastic optimization. *arXiv preprint arXiv:1412.6980*, 2014. 7
- [17] Yumeng Li, Margret Keuper, Dan Zhang, and Anna Khoreva. Divide & bind your attention for improved generative semantic nursing. In *34th British Machine Vision Conference 2023, BMVC 2023*, 2023. 3
- [18] Zhiqiu Lin, Deepak Pathak, Baiqi Li, Jiayao Li, Xide Xia, Graham Neubig, Pengchuan Zhang, and Deva Ramanan. Evaluating text-to-visual generation with image-to-text generation. In *European Conference on Computer Vision*, pages 366–384. Springer, 2025. 2, 3, 5
- [19] Bingyan Liu, Chengyu Wang, Tingfeng Cao, Kui Jia, and Jun Huang. Towards understanding cross and self-attention in stable diffusion for text-guided image editing. In *Proceedings of the IEEE/CVF Conference on Computer Vision and Pattern Recognition*, pages 7817–7826, 2024. 1
- [20] Haotian Liu, Chunyuan Li, Qingyang Wu, and Yong Jae Lee. Visual instruction tuning. *Advances in neural information processing systems*, 36, 2024. 5
- [21] Nan Liu, Shuang Li, Yilun Du, Antonio Torralba, and Joshua B Tenenbaum. Compositional visual generation with composable diffusion models. In *European Conference on Computer Vision*, pages 423–439. Springer, 2022. 3
- [22] Vivian Liu and Lydia B Chilton. Design guidelines for prompt engineering text-to-image generative models. In *Proceedings of the 2022 CHI conference on human factors in computing systems*, pages 1–23, 2022. 1
- [23] Aleksander Madry. Towards deep learning models resistant to adversarial attacks. *arXiv preprint arXiv:1706.06083*, 2017. 7

- [24] Boming Miao, Chunxiao Li, Yao Zhu, Weixiang Sun, Zizhe Wang, Xiaoyi Wang, and Chuanlong Xie. Advlogo: Adversarial patch attack against object detectors based on diffusion models. *arXiv preprint arXiv:2409.07002*, 2024. 4
- [25] Alex Nichol, Prafulla Dhariwal, Aditya Ramesh, Pranav Shyam, Pamela Mishkin, Bob McGrew, Ilya Sutskever, and Mark Chen. Glide: Towards photorealistic image generation and editing with text-guided diffusion models. *arXiv preprint arXiv:2112.10741*, 2021. 2
- [26] Nikita Pavlichenko and Dmitry Ustalov. Best prompts for text-to-image models and how to find them. In *Proceedings of the 46th International ACM SIGIR Conference on Research and Development in Information Retrieval*, pages 2067–2071, 2023. 1
- [27] William Peebles and Saining Xie. Scalable diffusion models with transformers. In *Proceedings of the IEEE/CVF International Conference on Computer Vision*, pages 4195–4205, 2023. 1
- [28] Alec Radford, Jong Wook Kim, Chris Hallacy, Aditya Ramesh, Gabriel Goh, Sandhini Agarwal, Girish Sastry, Amanda Askell, Pamela Mishkin, Jack Clark, et al. Learning transferable visual models from natural language supervision. In *International conference on machine learning*, pages 8748–8763. PMLR, 2021. 5
- [29] Aditya Ramesh, Mikhail Pavlov, Gabriel Goh, Scott Gray, Chelsea Voss, Alec Radford, Mark Chen, and Ilya Sutskever. Zero-shot text-to-image generation. In *International conference on machine learning*, pages 8821–8831. Pmlr, 2021. 2
- [30] Aditya Ramesh, Prafulla Dhariwal, Alex Nichol, Casey Chu, and Mark Chen. Hierarchical text-conditional image generation with clip latents. *arXiv preprint arXiv:2204.06125*, 1(2):3, 2022. 1, 2
- [31] Robin Rombach, Andreas Blattmann, Dominik Lorenz, Patrick Esser, and Björn Ommer. High-resolution image synthesis with latent diffusion models. In *Proceedings of the IEEE/CVF conference on computer vision and pattern recognition*, pages 10684–10695, 2022. 1, 5
- [32] Olaf Ronneberger, Philipp Fischer, and Thomas Brox. U-net: Convolutional networks for biomedical image segmentation. In *Medical image computing and computer-assisted intervention—MICCAI 2015: 18th international conference, Munich, Germany, October 5-9, 2015, proceedings, part III 18*, pages 234–241. Springer, 2015. 1
- [33] Chitwan Saharia, William Chan, Saurabh Saxena, Lala Li, Jay Whang, Emily L Denton, Kamyar Ghasemipour, Raphael Gontijo Lopes, Burcu Karagol Ayan, Tim Salimans, et al. Photorealistic text-to-image diffusion models with deep language understanding. *Advances in neural information processing systems*, 35:36479–36494, 2022. 1, 2
- [34] Eyal Segalis, Dani Valevski, Danny Lumen, Yossi Matias, and Yaniv Leviathan. A picture is worth a thousand words: Principled recaptioning improves image generation. *arXiv preprint arXiv:2310.16656*, 2023. 3
- [35] Chenyang Si, Ziqi Huang, Yuming Jiang, and Ziwei Liu. Freeu: Free lunch in diffusion u-net. In *Proceedings of the IEEE/CVF Conference on Computer Vision and Pattern Recognition*, pages 4733–4743, 2024. 3
- [36] Jascha Sohl-Dickstein, Eric Weiss, Niru Maheswaranathan, and Surya Ganguli. Deep unsupervised learning using nonequilibrium thermodynamics. In *International conference on machine learning*, pages 2256–2265. PMLR, 2015. 2
- [37] Jiaming Song, Chenlin Meng, and Stefano Ermon. Denoising diffusion implicit models. *arXiv preprint arXiv:2010.02502*, 2020. 3
- [38] Yang Song, Jascha Sohl-Dickstein, Diederik P Kingma, Abhishek Kumar, Stefano Ermon, and Ben Poole. Score-based generative modeling through stochastic differential equations. *arXiv preprint arXiv:2011.13456*, 2020. 2
- [39] Ming Tao, Hao Tang, Fei Wu, Xiao-Yuan Jing, Bing-Kun Bao, and Changsheng Xu. Df-gan: A simple and effective baseline for text-to-image synthesis. In *Proceedings of the IEEE/CVF conference on computer vision and pattern recognition*, pages 16515–16525, 2022. 2
- [40] Yunlong Wang, Shuyuan Shen, and Brian Y Lim. Reprompt: Automatic prompt editing to refine ai-generative art towards precise expressions. In *Proceedings of the 2023 CHI conference on human factors in computing systems*, pages 1–29, 2023. 1
- [41] Tao Xu, Pengchuan Zhang, Qiuyuan Huang, Han Zhang, Zhe Gan, Xiaolei Huang, and Xiaodong He. AttnGAN: Fine-grained text to image generation with attentional generative adversarial networks. In *Proceedings of the IEEE conference on computer vision and pattern recognition*, pages 1316–1324, 2018. 2
- [42] Zeyue Xue, Guanglu Song, Qiushan Guo, Boxiao Liu, Zhuofan Zong, Yu Liu, and Ping Luo. Raphael: Text-to-image generation via large mixture of diffusion paths. *Advances in Neural Information Processing Systems*, 36, 2024. 1, 3
- [43] Jiahui Yu, Yuanzhong Xu, Jing Yu Koh, Thang Luong, Gunjan Baid, Zirui Wang, Vijay Vasudevan, Alexander Ku, Yinfei Yang, Burcu Karagol Ayan, et al. Scaling autoregressive models for content-rich text-to-image generation. *arXiv preprint arXiv:2206.10789*, 2(3):5, 2022. 2
- [44] Han Zhang, Tao Xu, Hongsheng Li, Shaoting Zhang, Xiaogang Wang, Xiaolei Huang, and Dimitris N Metaxas. StackGAN: Text to photo-realistic image synthesis with stacked generative adversarial networks. In *Proceedings of the IEEE international conference on computer vision*, pages 5907–5915, 2017. 2
- [45] Han Zhang, Jing Yu Koh, Jason Baldridge, Honglak Lee, and Yinfei Yang. Cross-modal contrastive learning for text-to-image generation. In *Proceedings of the IEEE/CVF conference on computer vision and pattern recognition*, pages 833–842, 2021.
- [46] Minfeng Zhu, Pingbo Pan, Wei Chen, and Yi Yang. Dm-gan: Dynamic memory generative adversarial networks for text-to-image synthesis. In *Proceedings of the IEEE/CVF conference on computer vision and pattern recognition*, pages 5802–5810, 2019. 2

A. Theoretical Analysis

In this section, we present the proof of the inequality $\|\nabla_{\xi}^2 s(\xi)\|_2 \stackrel{a.e.}{\leq} c$. First, we prove that this inequality holds within the domain of the function $s(\cdot)$. Then, we prove that the region where the derivatives of the function are undefined forms a set of zero measure, which guarantees the effectiveness of our method.

Proof of the inequality. Considering a neural network $f(\cdot)$ with the following structure:

$$f(x) = g_k(\omega_k \cdots g_1(\omega_1 x + b_1) + b_2 \cdots + b_k), \quad (16)$$

where x is the input, $g_i(\cdot)$ is the activation function for the i -th layer, ω_i is the weight matrix, and b_i is the bias vector for the i -th layer. Using the chain rule, the first derivative of $f(x)$ can be expressed by:

$$f'(x) = \frac{\partial g_k}{\partial z_k} \cdot \frac{\partial z_k}{\partial x} \quad (17)$$

where $z_k = \omega_k g_{k-1}(z_{k-1}) + b_k$. The second derivative is given by:

$$f''(x) = \frac{\partial^2 g_k}{\partial z_k^2} \cdot \left(\frac{\partial z_k}{\partial x}\right)^2 + \frac{\partial g_k}{\partial z_k} \cdot \frac{\partial^2 z_k}{\partial x^2}. \quad (18)$$

The complexity of the derivative mainly comes from the activation functions, as the first derivative of a linear function is constant and its second derivative is zero. Table. 1 presents the bounds of the first and second derivatives for basic activation functions widely used in neural networks. For smooth functions, both their first and second derivatives are bounded over the entire domain. For non-smooth activation functions, their first and second derivatives are bounded within the domain where they are defined. Let \mathbf{R} represent the entire space and define the domain of the second derivative of f as follows:

$$\text{dom}(g'') = \text{dom}(g_1'') \cap \text{dom}(g_2'') \cap \cdots \cap \text{dom}(g_k''). \quad (19)$$

Therefore, for any given $z \in \text{dom}(g'')$, we have the following bounds:

$$\|g_i'(z)\|_2 \leq M_i, \quad \|g_i''(z)\|_2 \leq C_i, \quad \|\omega_i\|_2 \leq W_i, \quad (20)$$

where $M_i, C_i, W_i, i = 1, \dots, k$, are positive constants. The first derivative of z_k with respect to x in terms of z_{k-1} can be expressed as:

$$\frac{\partial z_k}{\partial x} = \omega_k \cdot \text{diag}(g_{k-1}'(z_{k-1})) \cdot \frac{\partial z_{k-1}}{\partial x}. \quad (21)$$

And the second derivative of z_k with respect to x in terms of z_{k-1} can be expressed as:

$$\begin{aligned} \frac{\partial^2 z_k}{\partial x^2} &= \omega_k \cdot \left[\text{diag}(g_{k-1}''(z_{k-1})) \cdot \left(\frac{\partial z_{k-1}}{\partial x}\right)^2 \right] \\ &+ \omega_k \cdot \left[\text{diag}(g_{k-1}'(z_{k-1})) \cdot \frac{\partial^2 z_{k-1}}{\partial x^2} \right]. \end{aligned} \quad (22)$$

Now we use the recursive method to prove that f'' is bounded. For the derivative at the first layer:

$$\left\| \frac{\partial z_1}{\partial x} \right\|_2 = \|\omega_1\|_2 \leq W_1, \quad \left\| \frac{\partial^2 z_1}{\partial x^2} \right\|_2 = 0. \quad (23)$$

Assume that for z_{i-1} , its first and second derivatives are bounded:

$$\left\| \frac{\partial z_{i-1}}{\partial x} \right\|_2 \leq U_{i-1}, \quad \left\| \frac{\partial^2 z_{i-1}}{\partial x^2} \right\|_2 \leq V_{i-1}. \quad (24)$$

Then the first derivative of the i -th layer satisfies:

$$\begin{aligned} \left\| \frac{\partial z_i}{\partial x} \right\|_2 &\leq \|\omega_i\|_2 \cdot \|g_{i-1}'(z_{i-1})\|_2 \cdot \left\| \frac{\partial z_{i-1}}{\partial x} \right\|_2 \\ &= W_i \cdot M_{i-1} \cdot U_{i-1}. \end{aligned} \quad (25)$$

The second derivative also satisfies:

$$\begin{aligned} \left\| \frac{\partial^2 z_i}{\partial x^2} \right\|_2 &\leq \|\omega_i\|_2 \cdot \|g_{i-1}''(z_{i-1})\|_2 \cdot \left\| \frac{\partial z_{i-1}}{\partial x} \right\|_2^2 \\ &+ \|\omega_i\|_2 \cdot \|g_{i-1}'(z_{i-1})\|_2 \cdot \left\| \frac{\partial^2 z_{i-1}}{\partial x^2} \right\|_2 \\ &= W_i \cdot (C_{i-1} \cdot U_{i-1}^2 + M_{i-1} \cdot V_{i-1}). \end{aligned} \quad (26)$$

Let

$$\begin{aligned} U_i &= W_i \cdot M_{i-1} \cdot U_{i-1}, \\ V_i &= W_i \cdot (C_{i-1} \cdot U_{i-1}^2 + M_{i-1} \cdot V_{i-1}), \end{aligned} \quad (27)$$

then we have:

$$\left\| \frac{\partial z_i}{\partial x} \right\|_2 \leq U_i, \quad \left\| \frac{\partial^2 z_i}{\partial x^2} \right\|_2 \leq V_i. \quad (28)$$

In this way we have proven that $f''(x)$ is bounded within its domain $\text{dom}(g'')$.

Proof that the inequality holds almost everywhere. Let $\mu(\cdot)$ denote the measure of sets, then we need to prove $\mu(\text{dom}(g'')) = \mu(\mathbf{R})$. Reviewing those non-smooth activation functions, their derivatives are only undefined at specific points, and the set of such points is very sparse in high-dimensional space. Take ReLU as an example. The points where its derivative is not defined occur only when the input is zero or when the input is mapped to zero after a linear transformation. Given that the weights in neural networks are typically close to full rank, the set of inputs where ReLU's derivative is undefined forms a lower-dimensional manifold, which is sparse in high-dimensional space. Consequently, the measure of this set is zero. Therefore $\mu(\mathbf{R} \setminus \text{dom}(g_i'')) = 0, i = 1, \dots, k$. Since

$$\mathbf{R} \setminus \text{dom}(g'') = (\mathbf{R} \setminus \text{dom}(g_1'')) \cup \cdots \cup (\mathbf{R} \setminus \text{dom}(g_k'')), \quad (29)$$

Activation Function	Mathematical Form	First Order Derivative Properties	Second Order Derivative Properties
ReLU	$g(x) = \max(0, x)$	$g'(x) = 1 \cdot I(x > 0) + 0 \cdot I(x < 0)$	$g''(x) = 0$ (except at $x = 0$)
Sigmoid	$g(x) = \frac{1}{1+e^{-x}}$	$ g'(x) \leq \frac{1}{4}$	$ g''(x) \leq \frac{1}{4}$
Tanh	$g(x) = \frac{e^x - e^{-x}}{e^x + e^{-x}}$	$ g'(x) \leq 1$	$ g''(x) \leq 2$
Leaky ReLU	$g(x) = x \cdot I(x > 0) + \alpha x \cdot I(x \leq 0)$	$g'(x) = 1 \cdot I(x > 0) + \alpha \cdot I(x < 0)$	$g''(x) = 0$ (except at $x = 0$)
Swish	$g(x) = x \cdot \frac{1}{1+e^{-x}}$	$ g'(x) < 2$	$ g''(x) < 2$
ELU	$g(x) = x \cdot I(x > 0) + \alpha(e^x - 1) \cdot I(x \leq 0)$	$ g'(x) \leq \max(0, \alpha)$	$g''(x) \leq \alpha $ (except at $x = 0$)
GELU	$g(x) = x \cdot \Phi(x)$	$ g'(x) \leq 1$	$ g''(x) \leq 0.5$
Mish	$g(x) = x \cdot \tanh(\ln(1 + e^x))$	$ g'(x) \leq 1.5$	$ g''(x) \leq 2$
Softplus	$g(x) = \ln(1 + e^x)$	$ g'(x) \leq 1$	$ g''(x) \leq \frac{1}{4}$
Softmax	$g_i(x) = \frac{e^{x_i}}{\sum_j e^{x_j}}$	$ g'_i(x) \leq 1$	$ g''_i(x) \leq 1$

Table 1. Properties of commonly used activation functions and their first and second derivatives.

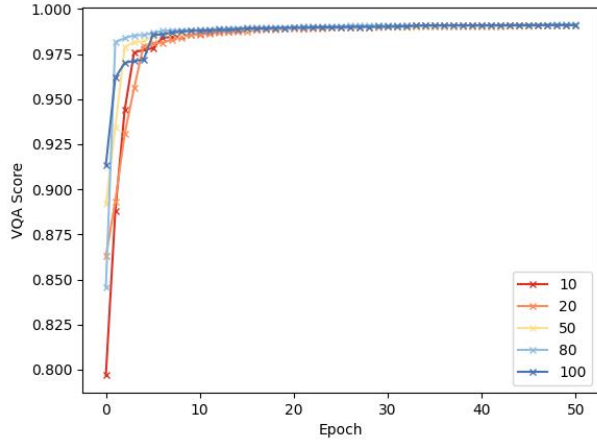


Figure 9. The average VQA score of the generated images across different epochs under various settings of the number of denoising timesteps.

then we can obtain that

$$\begin{aligned} \mu(\mathbf{R} \setminus \text{dom}(g'')) &\leq \mu(\mathbf{R} \setminus \text{dom}(g'_1)) + \dots \\ &+ \mu(\mathbf{R} \setminus \text{dom}(g'_k)) = 0. \end{aligned} \quad (30)$$

Therefore, we can conclude that the region where f'' is un-defined forms a set of measure zero, and the inequality for f'' is satisfied almost everywhere. Therefore, the function $s(\cdot)$ used to compute the score of latent variables in this paper also satisfies this condition, meaning that there exists a constant c so that for any ξ in the Gaussian space, we have $\|\nabla_{\xi}^2 s(\xi)\|_2 \leq c$ almost everywhere.

B. Hyper-parameters

B.1. Number of Denoising Timesteps

To investigate the impact of the number of denoising timesteps T . We select the cases of $T = 10, 20, 50, 80, 100$ and use the prompt “an apple and a pear” as an example, conducting the experiment with 25 random seeds. The quantitative results are shown in Fig. 9. Regardless of the number of timesteps, our method consistently leads to significant improvements. Generally speaking, increasing the

number of timesteps can enhance the VQA score of the initial images; however, the VQA score after increasing the timesteps still leaves room for improvement. Fig. 10 shows an extreme example: increasing T from 10 to 100 does not result in a substantial change in the image content. In contrast, after optimizing the noisy latent variable, the generated images have a significant improvement in alignment with the prompt across different settings. This demonstrates that our method enhances the faithfulness across different numbers of timesteps. When it comes to the choice of T , selecting smaller values can significantly speed up inference time while still yielding satisfactory images. If speed is the primary concern, one could opt for $T = 20$ or even $T = 10$. However, to balance stability with performance, $T = 50$ is a recommended choice based on the current performance of diffusion models.

B.2. Number of Candidate Noises

The number of candidate noises N should be large enough to ensure that the optimization progresses in the direction of increasing the VQA score. Since the latent variable exists in a high-dimensional space, it is unlikely to find a noise that leads to the step difference perfectly aligning with the gradient through random sampling. Instead, the criterion for setting N is to ensure that the lower bound is sufficiently large. We set N to different values: 10, 20, 50, 80 and 100, and observe the statistical characteristics of $\nabla_{z_T} s(z_T)v/\|v\|_2^2$ under these settings. As shown in Fig. 11, when N increases from 10 to 20, the lower quartile (Q1) improves from 0.026 to 0.035. When N reaches 50, it further increases to 0.043, demonstrating the effect of increasing the number of candidate noises. As N increases to 100, Q1 reaches 0.048. Although the rate of improvement begins to slow down, increasing N further will still lead to continued growth. Therefore, although we set N as 50 in our experiments, increasing N undoubtedly has a positive effect on the optimization.

C. Datasets

We present the prompt datasets used in our main experiment. Table. 2 shows the dataset for simple cases, which in-

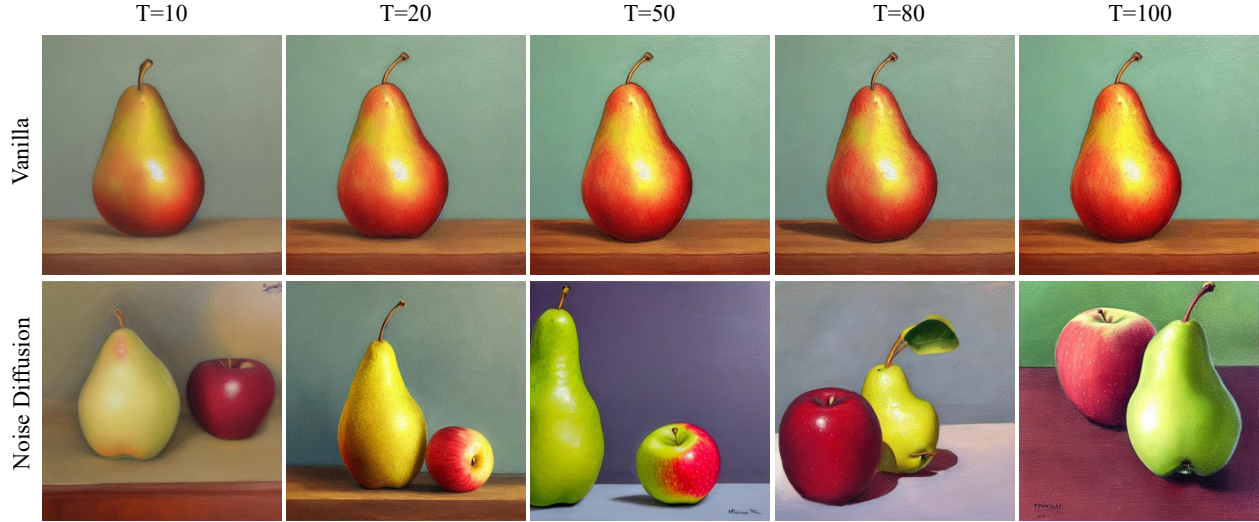


Figure 10. An example of an extreme case. Increasing the number of denoising timesteps does not lead to an improvement in the alignment of the generated image with the prompt. However, under different settings of the number of timesteps, our method consistently enhances the faithfulness.

an elephant and a rabbit a bird and a lion a dog and an elephant a cat and a bird a dog and a rabbit a dog and a rabbit a horse and a frog a lion and a frog a cat and a lion a bird and a frog a monkey and a mouse a horse with a glasses a bird with a crown a turtle and a gray backpack a rabbit and a orange backpack a bear and a blue clock a horse and a pink balloon a horse and a blue backpack a turtle and a pink balloon a monkey and a blue chair a lion and a black backpack a monkey with a bow an elephant and a yellow clock a bird and a yellow car a horse with a bow a horse and a green suitcase a mouse with a glasses a lion and a white bench an elephant and a pink backpack a rabbit and a yellow suitcase a rabbit and a gray clock a rabbit with a bow an elephant and a brown car a cat with a crown a monkey with a glasses a pink crown and a purple bow a green glasses and a black crown a yellow backpack and a purple chair a blue balloon and a blue bow a yellow glasses and a brown bow a green backpack and a yellow crown a green bench and a red apple a purple car and a pink apple a black backpack and a pink balloon a green backpack and a brown suitcase a pink chair and a gray apple	a dog and a frog a lion and a monkey a dog and a horse a dog and a monkey a bird and a rabbit a cat and a bear a cat and a horse a frog and a horse a lion and a rabbit a lion and a horse a cat and a frog a bear with a glasses a turtle and a yellow bowl an elephant and a green balloon a rabbit and a orange apple a cat and a gray bench a turtle and a yellow car a frog with a bow a cat and a red apple a turtle and a blue chair a dog with a crown a mouse and a blue clock a bird and a green chair a frog and a orange car a bird and a yellow apple an elephant with a crown a horse and a brown bowl a rabbit and a gray bowl a lion and a orange suitcase a horse and a blue bench a bear and a pink apple a mouse and a pink suitcase a turtle with a glasses a rabbit and a yellow car a frog with a glasses a blue clock and a blue apple a purple chair and a red bow a gray backpack and a green clock a white bow and a white car a red glasses and a red suitcase a orange glasses and a pink clock a gray backpack and a yellow glasses a gray crown and a purple apple a blue suitcase and a gray balloon a green glasses and a black bench a yellow suitcase and a yellow car	a bird and a mouse a horse and a turtle a turtle and a mouse a lion and a mouse an elephant and a turtle a rabbit and a horse a frog and a rabbit a dog and a mouse a cat and a monkey a bear and a horse a monkey and a turtle a monkey and a red car a rabbit and a gray chair a monkey and a orange apple a monkey and a green bowl a bear with a crown a lion with a glasses an elephant with a glasses a monkey and a brown bench a dog with a bow a horse and a green apple a bird and a black bowl a mouse and a black balloon a dog and a pink bench a monkey with a crown a monkey and a orange suitcase a monkey and a yellow clock a lion and a brown balloon an elephant and a orange apple a dog and a green suitcase a lion and a white chair a lion and a pink bowl a cat and a black suitcase a cat with a bow an elephant and a green bowl a blue balloon and a orange bench a yellow glasses and a black car a blue crown and a red balloon a orange bowl and a purple apple a pink bow and a gray apple a purple chair and a orange bowl a green glasses and a yellow chair a orange car and a red bench a yellow glasses and a gray bowl a white bow and a black clock a green backpack and a purple bench	a monkey and a frog a bird and a monkey a cat and a turtle a bear and a lion a lion and an elephant a rabbit and a mouse a bear and a mouse a lion and a rabbit a bear and a rabbit a bear and an elephant a horse and an elephant an elephant with a bow a dog and a black apple a lion and a red car a frog and a red suitcase a lion with a bow a cat and a yellow balloon an elephant and a black chair a rabbit with a glasses a dog and a gray clock a horse and a white car a turtle and a white bench a frog with a crown a cat and a blue backpack a turtle and an orange suitcase a turtle with a bow a horse and a pink chair an elephant and a green suitcase a mouse and a red car a rabbit with a crown a frog and a black chair a cat and a yellow car a bird and a white clock a bird with a glasses a pink crown and a red chair a orange backpack and a purple car a frog suitcase and a black bowl a brown chair and a white bench a gray crown and a white clock a orange suitcase and a brown bench a white glasses and a gray apple a red suitcase and a blue apple a white suitcase and a white chair a red crown and a black bowl a black crown and a red car	a horse and a monkey a bear and a frog a dog and a mouse a bird and an elephant a cat and a rabbit a lion and a bear a monkey and a rabbit an elephant and a rabbit a turtle and a rabbit a horse and a mouse a cat and a mouse a bear and a purple balloon a rabbit and a white bench a lion with a crown a monkey and a green balloon a bear and a red balloon a horse and a yellow clock a bird and a brown balloon a bear and a gray bench a mouse and a purple chair a dog and a purple car a mouse and a pink apple a bird with a bow a frog and a green bowl a turtle and a pink apple a lion and a gray apple a dog and a brown backpack an elephant and a green bench a horse with a crown a cat and a black chair a mouse and a purple bowl a frog and a green clock a frog and a yellow backpack a cat and a green clock a dog and a blue balloon a orange chair and a blue clock a white balloon and a white apple a brown balloon and a pink car a purple crown and a blue suitcase a black car and a white clock a white glasses and a orange balloon a gray suitcase and a brown bow a red backpack and a yellow bowl a purple crown and a blue bench a green chair and a purple car a green balloon and a pink bowl	a bird and a turtle a cat and an elephant a lion and a turtle a dog and a bear a bear and a monkey a cat and a dog a frog and a turtle an elephant and a monkey a dog and a turtle an elephant and a mouse a mouse with a bow a lion and a yellow clock a bird and a purple bench a cat with a glasses a bird and a black backpack a dog with a glasses a monkey and a yellow backpack a turtle and a blue clock a bear and a white car a dog and a gray bowl a bear and a orange backpack a turtle with a crown a frog and a pink bench a dog and a orange chair a mouse with a crown a cat and a purple bowl a rabbit and a white balloon a bear with a bow a bear and a red suitcase a frog and a black apple a bear and a white chair a bird and a black suitcase a bear and a purple bowl a mouse and a brown backpack a purple bowl and a black bench a brown suitcase and a black clock a black backpack and a green bow a yellow bow and a orange bench a brown bowl and a green clock a yellow backpack and a gray apple a white car and a black bowl a red bench and a yellow clock a yellow bow and a pink bowl a white chair and a gray balloon a purple balloon and a white clock
--	---	---	---	--	--

Table 2. Prompt dataset for simple cases.

cludes a total of 276 prompts, categorized into three groups: animals, animals-objects, and objects. The complex cases are shown in Table 3, where we have a total of 100 prompts, which similarly include animals, animals-objects and objects, but with additional spatial relationships such as “on,” “under,” “above,” and “below.” These added relationships

increase the complexity of the prompts, forcing text-to-image models to better understand and reflect the logical structure within the prompts.

an elephant under a rabbit a bird on a monkey a bird above an elephant a cat under a rabbit a cat on a horse a horse under a rabbit a monkey under a turtle a turtle under a yellow bowl a monkey above a green bowl a turtle below a blue clock a cat on a white bench a monkey on an orange suitcase a rabbit under a blue bowl a frog on a green clock a purple bowl on a black bench a purple crown on a blue suitcase a brown bowl below a green clock a green bench under a red apple a red suitcase under a blue apple a green backpack under a brown suitcase	a dog under a frog a dog on an elephant a lion under a turtle a dog on a bear a frog under a mouse a cat below a monkey a cat above a mouse a rabbit on a gray chair a bear below a blue clock a monkey on a blue chair a bird above a yellow car a mouse below a crown a dog above a green suitcase a pink crown under a purple bow an orange backpack on a purple car a yellow bow above an orange bench a green backpack under a yellow crown a gray suitcase under a brown bow a red backpack under a yellow bowl a white bow on a black clock	a monkey under a frog a cat on an elephant a dog below a bird a cat above a bear a dog on a lion an elephant below a monkey an elephant under a mouse a rabbit under a white bench a bear under a crown a bear below an orange backpack a monkey under a crown a horse under a brown bowl a cat under a black chair a blue clock under a blue apple a brown suitcase below a black clock a pink bow on a gray apple a purple chair under an orange bowl a white car under a black bowl a black backpack below a pink balloon a red crown under a black bowl	a bird on a turtle a dog under a monkey a bird above a rabbit a bird on a horse an elephant under a frog a bird above a frog a monkey on a red car a lion below a yellow clock a mouse under a red bench a bird on a green chair a cat above a blue backpack a monkey below a yellow clock a lion under a pink bowl a blue balloon on an orange bench a gray backpack under a green clock a gray crown below a white clock an orange suitcase under a brown bench a purple car under a pink apple a blue suitcase below a gray balloon a yellow suitcase on a yellow car	a bird above a lion a lion under a mouse an elephant under a turtle a bear under a monkey a cat on a lion a cat above a frog a frog below a purple balloon an elephant below a green balloon a bear under a gray bench a mouse below a black balloon a dog on an orange chair a lion on a white bench a frog on a black chair a pink crown under a red chair a brown balloon above a pink car a black car under a white clock a yellow backpack under a gray apple a gray crown under a purple apple a white suitcase on a white chair a green balloon above a pink bowl
--	---	--	---	---

Table 3. Prompt dataset for complex cases.

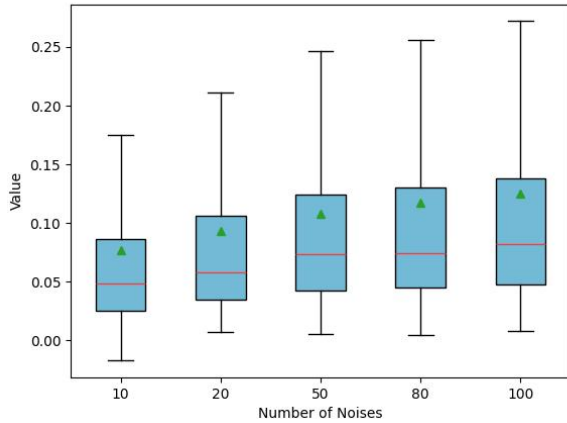


Figure 11. The statistical characteristics of $\nabla_{z_T} s(z_T)v/\|v\|_2^2$ with different values of N during the optimization.

D. More Results

We present additional results for vanilla settings and our method on SD V-1.4, V-1.5, V-2.0 and V-2.1 in Fig. 12, Fig. 13, Fig. 14 and Fig. 15, respectively.

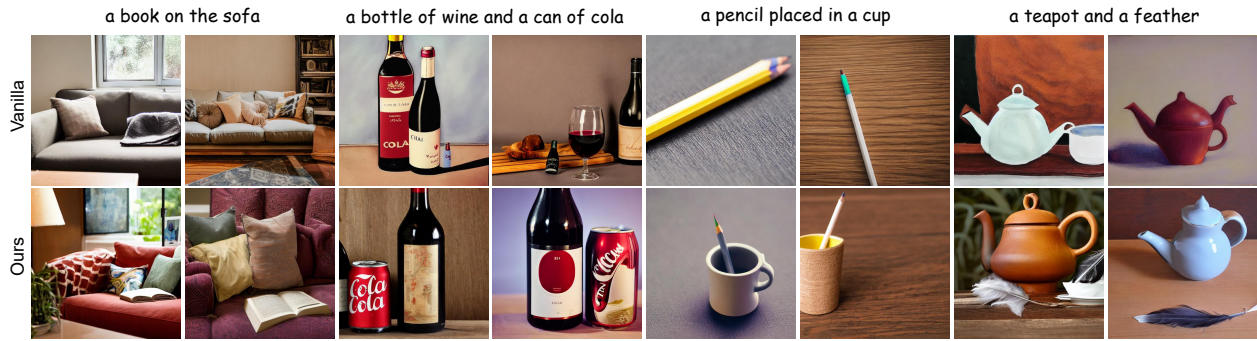


Figure 12. Outputs of Vanilla settings and our method for SD V-1.4.



Figure 13. Outputs of Vanilla settings and our method for SD V-1.5.



Figure 14. Outputs of Vanilla settings and our method for SD V-2.0.



Figure 15. Outputs of Vanilla settings and our method for SD V-2.1.